

Decoherence and Quantum Interference assisted electron trapping in a quantum dot

Ahmed El Halawany^{1,2} and Michael N. Leuenberger^{1,2*}

¹*NanoScience Technology Center, University of Central Florida, Orlando, Florida 32826, USA and*

²*Department of Physics, University of Central Florida, Orlando, Florida 32816, USA*

We present a theoretical model for the dynamics of an electron that gets trapped by means of decoherence and quantum interference in the central quantum dot (QD) of a semiconductor nanoring (NR) made of five QDs, between 100 K and 300 K. The electron's dynamics is described by a master equation with a Hamiltonian based on the tight-binding model, taking into account electron-LO phonon interaction (ELOPI). Based on this configuration, the probability to trap an electron with no decoherence is almost 27%. In contrast, the probability to trap an electron with decoherence is 70% at 100 K, 63% at 200 K and 58% at 300 K. Our model provides a novel method of trapping an electron at room temperature.

PACS numbers: 03.67.Bg, 73.23.Hk, 03.65.Yz, 81.07.Ta

I. INTRODUCTION

The interaction between a quantum system and its environment is inevitable, leading to decoherence,¹ which is one of the main obstacles in fields such as quantum information processing,² quantum optics, when measuring optical Schrödinger cat states,³ condensed matter physics, when looking for mesoscopic interference phenomena in quantum transport of electrons,^{4,5} etc. Since many interesting quantum phenomena are based on coherence, many solutions are proposed, and are currently in use, to suppress or overcome decoherence,⁶ such as quantum error-correction codes,⁷ error-avoiding codes,⁷ echo techniques,^{8,9} quantum feedback operations,³ optimal control technique,¹⁰ and many more. Other research groups are trying to fight decoherence through the knowledge of their spectral density, thinking this would be more operative.¹¹ A rather opposite approach to this stream of research is found in quantum biology, where scientists are trying to take advantage of the decoherence in the quantum dynamics of excitons in order to find explanations for the high efficiency in solar energy harvesting in photosynthetic systems.^{12,13} Recent explanations include environment-assisted energy transfer in quantum networks, such as noise-assisted transport^{12,14} and oscillation-enhanced transport.^{15,16}

The role of decoherence in localizing electrons has been reported in many previous works.^{17,18} Another approach is to apply continuous measurement to keep the quantum state in a pure state. This approach is known as the quantum Zeno effect.¹⁹ Some groups report that continuous measurement will lead to quantum anti-Zeno effect.²⁰ In all previous reports, quantum interference does not play any role in trapping the electron. In this work, we present a configuration that focuses on the interplay between quantum interference of the electron wavefunction and decoherence in trapping the electron in the central QD. Neither quantum interference nor decoherence alone can trap the electron wavefunction in one out of five coupled quantum dots. It is the combined effect of quantum interference and decoherence that leads to the trapping.

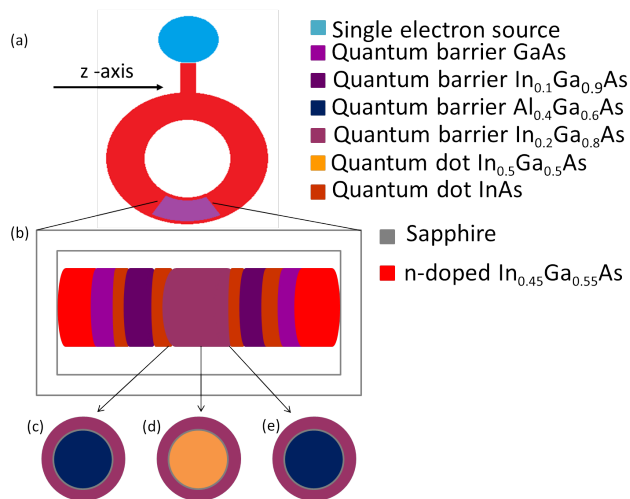


Figure 1: (a) Schematic setup (not to scale). (b) A magnified diagram for the intrinsic region made of five quantum dots of (from left to right) 1.24, 1.5, 5.0, 1.5, 3.14 nm height, respectively. (c) A cross section view for the interface between quantum dot #2 and barrier #3. (d) A cross section view for quantum dot #3 (electron pocket). (e) A cross section view for the interface between quantum dot #2 and barrier #4.

II. STRUCTURE AND MECHANISM

We consider the transport of a single electron in a NR with 15.1 nm as minor radius and 30 nm as major radius (see Fig. 1). The NR is divided into two regions. The first region, which is n-doped In_{0.45}Ga_{0.55}As with a concentration of $6.0 \times 10^{14} \text{ cm}^{-3}$, constitutes 85% of the NR, and it will be referred to as the "zero-region" in the manuscript. The second region is called the "intrinsic-region" in the manuscript. It consists of five QDs, four of which are made of InAs, and the central QD is made of In_{0.5}Ga_{0.5}As. QD #5, (see Fig. 2 for QDs labeling), is n-doped with a concentration of $1.0 \times 10^{18} \text{ cm}^{-3}$. The zero-region and QD #5 are not degenerate semiconductors. Barrier #1 and #6 are made of GaAs, while barriers #2 and #5 are made of In_{0.1}Ga_{0.9}As. As for barrier #3

and #4, they are made of $\text{Al}_{0.4}\text{Ga}_{0.6}\text{As}$. A monolayer of sapphire Al_2O_3 , which has radius of 8.05 nm, coats the region starting from the interface between QD #2 and barrier #3 to the interface of barrier #4 and QD #4. The outer layer, up to the surface of the NR, is made of $\text{In}_{0.2}\text{Ga}_{0.8}\text{As}$. As a result of this concentric configuration, the central QD acts like an *electron pocket* that traps the electron with the help of decoherence, as will be shown later. All interfaces between the materials considered in the aforementioned configuration are recognized to be straddling gaps (type I). Based on all chosen materials and types of interfaces, the conduction band (CB) profile is shown in Fig. 2, based on the self-consistent solution of the Schrödinger-Poisson equation. All semiconductor materials have the same crystal structure and direct band gap. In addition, the NR is coupled to a single-electron source (SES).^{21,22} The SES is triggered to emit an electron and thus this electron can transport through the whole configuration. Therefore, the time evolution is well described by the single-electron master equation as shown and justified below.

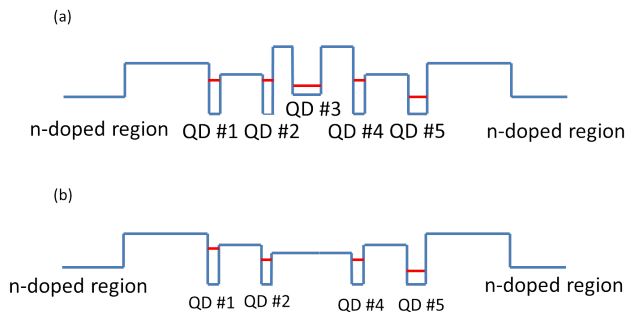


Figure 2: (a) The conduction band, for radius $r < 8.05$ nm. (b) The conduction band, for $r > 8.05$ nm. The quantum dots' ground eigenstates are shown.

III. MODEL

Given that the aforementioned configuration has zero electric field across the five-QD region and the electron's eigenenergies are close to the conduction band-edge minima, the 3D time-independent Schrödinger equation in cylindrical coordinates and in the effective mass approximation is used to find the eigenenergies and eigenstates for each QD separately. These states are used later (see below) to describe the dynamics of the electron by means of a generalized master equation in the tight-binding approximation, taking into account ELOPI. For simplicity, an infinite confining potential in the radial direction is assumed. The eigenenergies and wavefunctions of QDs #1 and #5 are obtained systematically. As for QD #3, due to the relatively large band gap (5 eV) for the sapphire Al_2O_3 monolayer, it is assumed to be confined in infinite potential but with different radius than QDs #1 and #5. Both QDs #2 and #4 (see App. B), require an

additional boundary condition due to the *electron pocket* i.e. the electron's energy has to be conserved irrespective of the interface with $\text{Al}_{0.4}\text{Ga}_{0.6}\text{As}$ or $\text{In}_{0.2}\text{Ga}_{0.8}\text{As}$ (see Fig. 1). The zero energy is set at the minimum of the conduction band of InAs QDs.

We start with the following Hamiltonian

$$H = H_I + H_c, \quad (1)$$

where H_I is the Hamiltonian of an electron in the "intrinsic-region"

$$H_I = \sum_i \varepsilon_i a_i^\dagger a_i + \left(- \sum_{i \neq j} t_{ij} a_i^\dagger a_j + \text{h.c.} \right) + \hbar\omega_{LO} b^\dagger b + \lambda \sum_i a_i^\dagger a_i (b^\dagger + b), \quad (2)$$

and H_c is the Hamiltonian that describes the coupling between both QD #1 and #5 and "zero-region"

$$H_c = \left(\sum_0 V_{01} C_0^\dagger a_1 + \text{h.c.} \right) + \left(\sum_0 V_{05} C_0^\dagger a_5 + \text{h.c.} \right). \quad (3)$$

In Eq. (2), the first term describes the on-site ground state for the five QDs. The second term, which is based on the tight-binding model, describes the hopping of the electron between the QDs, where t_{ij} is a 3-D hopping integral given by the off-diagonal matrix elements of H_t ,²³ i.e. (see Sec. IV for details)

$$t_{ij} = \int \Psi_i^* H_t \Psi_j d^3r, \quad (4)$$

where H_t is the kinetic and potential energy of the electron inside the QD,

$$H_t = -\frac{\hbar^2}{2m^*} \nabla_{3D}^2 + V(r, z). \quad (5)$$

The third term in Eq. (2) describes non-dispersive LO phonons of $\text{In}_{0.45}\text{Ga}_{0.55}\text{As}$, since it constitutes 85% of the NR. In polar semiconductors, as the size of the QD decreases, electrons interact mostly with phonons that have long wavelength $|\mathbf{q}| \leq 2\pi / (\text{QD size})$. This suggests that a model with dispersionless LO phonons is accurate.²⁴ It has been shown in experimental work that for InAs QDs embedded in GaAs matrix, the GaAs LO phonons are more prominent than the InAs LO phonons.²⁵ The fourth term in Eq. (2) describes the interaction between the electron and LO phonons with coupling strength λ (see App. A). In this work, $g = \lambda / (\hbar\omega_{LO}) \approx 0.066$. As for the acoustic phonons, in polar semiconductor nanostructures, the electron-acoustic phonon coupling is weak because the energy difference between the ground state and excited state ΔE is greater than 64 meV in all QDs. Moreover, in the central QD the energy difference is greater than 110 meV. As a result, the acoustic phonons are taken into account in the master equation, as shown later, as part of the total decoherence. Since we

deal with ELOPI, a canonical unitary transformation is useful to eliminate the linear coupling terms in Eq. (2). The transformed Hamiltonian is $H'_I = e^S H_I e^{-S}$, where $S = -g \left(\sum_i a_i^\dagger a_i (b^\dagger + b) \right)$. We obtain

$$\begin{aligned} H'_I = & \sum_i a_i^\dagger a_i (\varepsilon_i - \lambda^2 / \hbar \omega_{LO}) \\ & + \left(- \sum_{ij} t_{ij} a_i^\dagger a_j e^{-2g(b^\dagger - b)} \right) \\ & + \left(- \sum_{ij} t_{ji} a_j^\dagger a_i e^{2g(b^\dagger - b)} \right) \\ & + \hbar \omega_{LO} b^\dagger b + (2\lambda^2 / \hbar \omega_{LO}). \end{aligned} \quad (6)$$

In Eq. (6) the first term shows the renormalization of the QDs' eigenstates in the presence of ELOPI. The eigenstates of the transformed Hamiltonian H'_I are in the tensor product form and are denoted by $|\nu_g, N\rangle$ and $|\nu_e, N\rangle$, where ν_g and ν_e represent the ground and excited state of the electron in QD $\# \nu$, respectively, and N represents the number of LO phonons. The Hamiltonian in Eq. (6) is solved in the following basis $|SES\rangle$, $|zero - region\rangle$, $|1_g, 0\rangle$, $|2_g, 0\rangle$, $|3_g, 0\rangle$, $|4_g, 0\rangle$ and $|5_g, 0\rangle$, where $|SES\rangle$ is the electron in the SES before being injected in the NR, $|zero - region\rangle$ is the electron in the "zero-region" in the NR after being injected from the SES, and $|1_g, 0\rangle$ is the electron in the ground state of QD $\#1$ with no phonons. We define the phonon displacement operator $D(\beta) = e^{\beta b^\dagger - \beta^* b}$. We can now make use of the well-known formula for the matrix elements of the displacement operator^{26,27}

$$\begin{aligned} \langle N' | D(\beta) | N \rangle = & \left(\frac{N!}{N'} \right)^{1/2} |\beta|^{N'-N} e^{-|\beta|^2/2} \\ & \times L_N^{N'-N}(|\beta|^2) e^{i(N'-N)\phi}, \end{aligned} \quad (7)$$

where $\beta = |\beta| e^{i\phi}$ and $L_N^{N'-N}(|\beta|^2)$ are the associated Laguerre polynomials. For $\beta \ll 1$ the associated Laguerre polynomials are approximately

$$L_N^{N'-N}(|\beta|^2) \approx \frac{N!}{N!(N'-N)!} \left(1 + \frac{N}{N'-N+1} |\beta|^2 \right). \quad (8)$$

Thus, for $\beta \ll 1$ only the phonon states with $N' = N$ couple to each other in a good approximation, and $\langle N | D(2g) | N \rangle = e^{-2g^2}$. Therefore, the second and third terms in Eq. (6) show that the hopping term t_{ij} is reduced by a factor of $e^{-2\lambda^2 / (\hbar \omega_{LO})^2}$. In the weak ELOPI considered in this work, $e^{-2\lambda^2 / (\hbar \omega_{LO})^2} \approx 1$ and thus the hopping terms are not reduced (see App. A).

The validation of the aforementioned Hamiltonian depends on the following criteria; in this configuration there must be no electrons in the CB. This is calculated in the

standard way as follows

$$n = \int_{E_c}^{\infty} D(E) f^{FD}(E) dE. \quad (9)$$

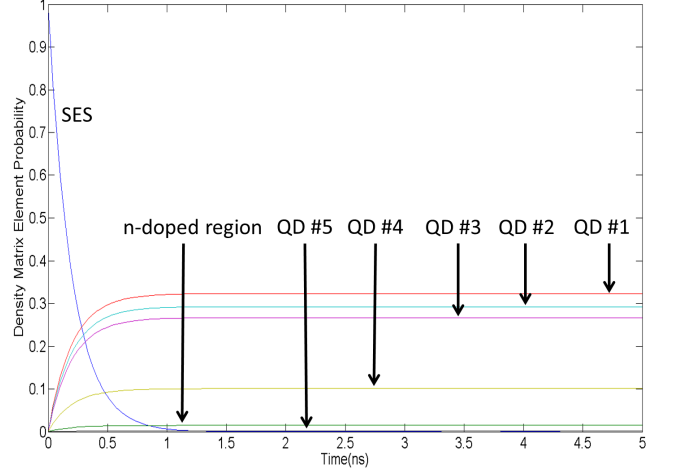


Figure 3: The electron's time-dependent probability distribution among the five quantum dots in the case with zero decoherence.

Since the configuration has a large length-to-width ratio, $D(E)$ is approximated by the density of states of a 1D NR (Section V). Doping (type and concentration) along with temperature are taken into account through the Fermi-Dirac function $f^{FD}(E)$. We observe that on average there are virtually no electrons in the whole configuration. Consequently, when the SES is triggered and a single electron is emitted, H'_I is a valid description for this single electron. H_c describes the coupling between the "zero-region" (quasi-continuum) and QDs $\#1$ and $\#5$. The electron inside the "zero-region" is incoherent because of the decoherence effects due to the acoustic phonons. Such effects do not conserve the energy of the electron. This coupling is well described by Fermi's golden rule for the transition rates as follows:

$$\begin{aligned} W_{0 \rightarrow 1_g} = & \frac{2\pi}{\hbar} \int_{E_c}^{\infty} dE_0 |\langle 1_g | H_c | 0 \rangle|^2 D(E_0) f^{FD}(E_0) \\ & \times (1 - f^{FD}(E_{1g})) \delta(E_{1g} - E_0), \end{aligned} \quad (10)$$

$$\begin{aligned} W_{1_g \rightarrow 0} = & \frac{2\pi}{\hbar} \int_{E_c}^{\infty} dE_0 |\langle 0 | H_c | 1_g \rangle|^2 D(E_0) f^{FD}(E_{1g}) \\ & \times (1 - f^{FD}(E_0)) \delta(E_{1g} - E_0), \end{aligned} \quad (11)$$

$$\begin{aligned} W_{5_g \rightarrow 0} = & \frac{2\pi}{\hbar} \int_{E_c}^{\infty} dE_0 |\langle 0 | H_c | 5_g \rangle|^2 D(E_0) f^{FD}(E_{5g}) \\ & \times (1 - f^{FD}(E_0)) \delta(E_0 - E_{5g}), \end{aligned} \quad (12)$$

and

$$\begin{aligned} W_{0 \rightarrow 5_g} = & \frac{2\pi}{\hbar} \int_{E_c}^{\infty} dE_0 |\langle 5_g | H_c | 0 \rangle|^2 D(E_{5g}) f^{FD}(E_0) \\ & \times (1 - f^{FD}(E_{5g})) \delta(E_0 - E_{5g}) \end{aligned} \quad (13)$$

The coupling terms in Eq. (3), V_n and V_p , are much smaller than t_{12} and t_{45} . This confirms that we have a weak coupling between the outer QDs and the "zero-region". Thus a standard formalism appropriate for the description of such a system is the generalized master equation in the Born and Markov approximation²⁸

$$\partial_t \rho_{m,n} = \frac{i}{\hbar} [\rho, H_I]_{m,n} + \delta_{m,n} \sum_{l \neq m} \rho_n W_{m,l} - \gamma_{m,n} \rho_{m,n}, \quad (14)$$

where $\gamma_{m,n} = \frac{1}{2} \sum_l (W_{l,n} + W_{l,m}) + \frac{1}{T_2}$ is the total decoherence which includes the dephasing time T_2 due to electron-phonon (both acoustic and optical, and both elastic and inelastic) interaction and the rates $W_{m,l}$ of transition between the "zero-region" and the outer QDs. Eq. (14) is valid when the correlation time in the heat bath is much smaller than the relaxation time of the electron system. A rough estimate for the correlation time is $\frac{\hbar}{k_B T} \sim (1 - 3.5) \times 10^{-14}$ s for $T = 100$ K - 300 K respectively, which is much smaller than the electron relaxation time, in such systems, $\sim 10^{-12}$ s. The dephasing time T_2 , based on temperature, is determined through the homogeneous broadening $2\hbar/T_2$.^{29,30} At room temperature, the dephasing times are of the order of 200-300 fs.²⁹⁻³¹ We choose $T_2 = 285$ fs at 300 K because there is no carrier-carrier interaction. At $T = 100$ K, the dephasing time is 2 ps.²⁹⁻³¹ It is worth to mention that we ignore the change in band gap due to the lattice constant mismatch between the different materials. However, this does not affect the final results. For calculating the ground state of QD #5 the doping is taken into account through the Schrödinger-Poisson equation. As a result, the ground state of QD #5 will be $E'_{5g} = E_{5g} - \frac{\lambda^2}{\hbar\omega_{LO}} + \Delta$, where Δ is the increase in the ground energy of QD #5 (few meV) due to doping. The change in wavefunction of QD #5 is negligibly small. In this work only the ground state in each QD # ν , denoted by $|\nu_g, 0\rangle$, is considered. Such contribution is attributed to the following reasons; first, the electron's transition from the "zero-region" to the ground state $|1_g, 0\rangle$ is 100 times faster than the transition to the excited state $|1_e, 0\rangle$. In addition, the transition to $|5_g, 0\rangle$ is 10 times less than the transition to $|1_g, 0\rangle$. As a result, the electron in the "zero-region" will basically favor tunneling toward QD #1 more than QD#5. Second, in systems where the energy separation is 44 meV the relaxation takes 20 (40) ps at 300 (100) K.³² Thus, based on the detailed balance condition, $\frac{W_{nm}}{W_{mn}} = e^{-\frac{\hbar\omega_{nm}}{k_B T}}$, phonon-assisted excitation will take much more time. In addition, in the aforementioned configuration, based on the dimensions of the QDs, the energy separation is more than 64 meV. Third, in polar semiconductors, even at room temperature, the emission of LO phonon is more favorable than the absorption of LO phonon. As a result, the $|\nu_g, 0\rangle$ states remain populated and the excited states can be neglected.

In this model, we calculate all ten hopping integrals (Section IV). Based on the *electron pocket* configuration, t_{24} is larger than $t_{43} + t_{32}$. This is impossible to achieve

in a similar configuration without an *electron pocket*.

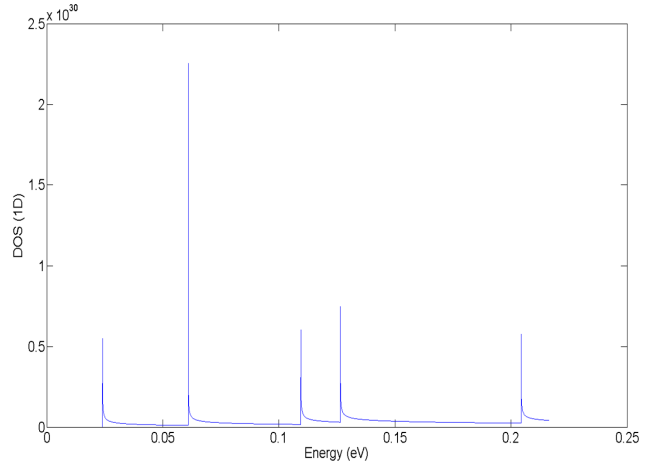


Figure 4: Density of states for a circular nanowire with radius of 15.1 nm.

IV. CALCULATION OF HOPPING MATRIX ELEMENTS

The total Hamiltonian of our system is

$$H_t = -\frac{\hbar^2}{2m^*} \nabla_{3D}^2 + V(r, z), \quad (15)$$

where the first term is the kinetic energy and the second term is the potential energy

$$V(r, z) = \sum_{\nu} V_{\nu}. \quad (16)$$

The potential V_{ν} represents the local potential of the QD # ν . This representation can be used to derive the tight-binding Hamiltonian H_I given in Eq. (2) for the "intrinsic-region". We provide an approximation to H_I in App. E. The diagonal and off-diagonal elements of H_t are given by

$$\epsilon_i = -\int \Psi_i^* \frac{\hbar^2}{2m^*} \nabla_{3D}^2 \Psi_i d^3r + \int \Psi_i^* V_i \Psi_i d^3r \quad (17)$$

and

$$t_{ij} = -\int \Psi_i^* \frac{\hbar^2}{2m^*} \nabla_{3D}^2 \Psi_j d^3r + \int \Psi_i^* V_i \Psi_j d^3r, \quad (18)$$

respectively. These are the variables that enter the tight-binding Hamiltonian H_I in Eq. (2). Due to the cylindrical symmetry of the QDs we can write the wavefunction as

$$\Psi = R(\rho) \Phi(\phi) Z(z). \quad (19)$$

Since the hopping is only along the axial axis (z-axis), H_t is

$$H_t = -\frac{\hbar^2}{2m^*} \partial_{zz} + V(r, z). \quad (20)$$

The hopping integral is calculated in the following manner

$$t_{ij} = \int R_i^*(\rho) \Phi_i^*(\phi) Z_i^*(z) H_t R_j(\rho) \Phi_j(\phi) Z_j(z) d^3r, \quad (21)$$

separating variables will yield

$$t_{ij} = \int_0^{2\pi} \Phi_i^*(\phi) \Phi_j(\phi) d\phi \int_0^r R_i^*(\rho) R_j(\rho) d\rho \times \int_{-\infty}^{\infty} Z_i^*(z) H_t Z_j(z) dz. \quad (22)$$

The azimuthal part will always result in 1. The azimuthal part acts like a selection rule for the electron hopping. The electron, in the considered configuration, hops between states with the same quantum number m . Consequently, the hopping occurs among the ground states of the QDs only. The radial integral requires special care, especially when one of the hopping integral's boundaries is located at the interface with the *electron pocket*,

$$\int_0^{\gamma r} R_{iin}^* R_{jin} dr + \int_{\gamma r}^r R_{iout}^* R_{jout} dr. \quad (23)$$

Since H'_I is a hermitian, $t_{ij} = t_{ji}^*$. The values of the hopping integral vary based on the QDs. They are $t_{21} = t_{12} = 161$ meV, $t_{54} = t_{45} = 180$ meV, $t_{31} = t_{13} = 14$ meV, $t_{53} = t_{35} = 5$ meV, $t_{41} = t_{14} = 24$ meV, $t_{25} = t_{52} = 0.464$ meV, $t_{51} = t_{15} = 0.1047$ meV, $t_{32} = t_{23} = 56.44$ meV, $t_{34} = t_{43} = 18.6$ meV, and $t_{42} = t_{24} = 85.7$ meV.

V. DENSITY OF STATES IN N-DOPED REGION

In this work, the NR's minor radius is 15.1 nm, and with circumference of almost 190 nm. The length-to-width ratio is almost 7 justifying the 1-D density of states (DOS) employed in this work. The DOS is given by³³

$$\rho^{1D}(E) = \sum_{i=1}^n \left(\frac{2m^*}{\hbar^2} \right)^{1/2} \frac{1}{\pi (E - E_i)^{1/2}} \Theta(E - E_i). \quad (24)$$

where Θ is a step function. The DOS graph is plotted in Fig. 4.

VI. RESULTS AND DISCUSSION

In the numerical calculations based on Eq. (14) the trace of the density matrix is equal to one at all times. This ensures probability conservation, which agrees with the Hamiltonian being hermitian. In Fig. 3, 5, 6, and 7 at

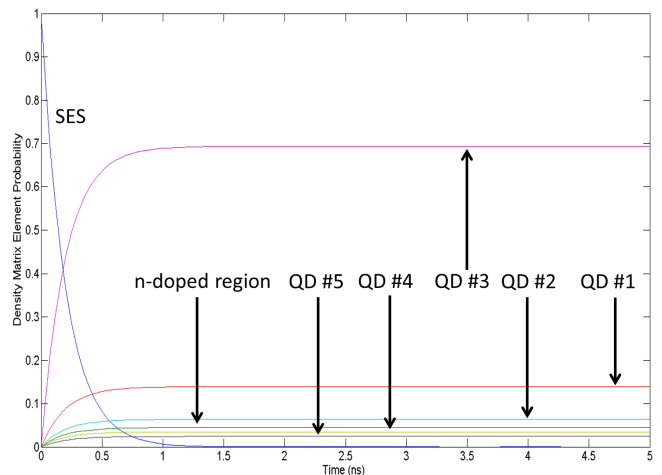


Figure 5: The electron's time-dependent probability distribution among the five quantum dots at 100 K. The probability to trap the electron in QD #3 is 70%.

$t = 0$, $\rho_{SES} = 1$, which means that there is no electron initially in the NR configuration. In addition, if decoherence is absent, the probability of the electron to get trapped in the central QD is 27%, as shown in Fig. 3. In contrast, if decoherence is taken into account, the electron's trapping probability increases to 58% - 70% depending on the temperature (see Figs. 5, 6, and 7). The probability of the electron's trapping at different temperatures and their corresponding dephasing times are shown in Table I.

Temperature [K]	Dephasing time T_2 [21]	Electron trap [%]
100	2 ps	70
150	667 fs	65
200	500 fs	63
250	334 fs	60
300	285 fs	58

Table I: Probability of electron being trapped in the central quantum dot at various temperatures between 100 K and 300 K.

Although the trapping probability decreases with increasing dephasing rate, it is larger than the trapping probability in the case of vanishing decoherence. Many factors contribute to this counter-intuitive result. The first factor is the *electron pocket*, which is essential for the electron to get accumulated in the central QD. To show the importance of the *electron pocket*, consider the following configuration where there is no *electron pocket* (i.e. $t_{42} < t_{43}$ and t_{32}). The electron is delocalized among all five QDs. In Fig. 8, the same eigenenergies and the same hopping matrix elements values were considered except for t_{42} . The result is due to the detuning of the energy levels of the QDs. However, there is no significant localization of the electron in QD #3.

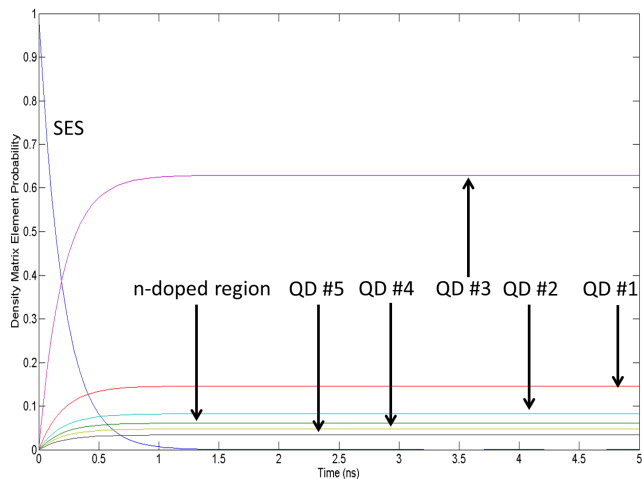


Figure 6: The electron's time-dependent probability distribution among the five quantum dots at 200 K. The probability to trap the electron in QD #3 is 63%.

The second factor is the fast electron transition from the "zero-region" to QD #1 and from QD #5 to the "zero-region". The electron's transition rate from the "zero-region" to the first QD's ground state $W_{0 \rightarrow 1g}$ is almost 100 times larger than $W_{1g \rightarrow 0}$. The electron's transition rate from the ground state of QD #5 to the "zero-region" $W_{5g \rightarrow 0}$ is almost 10 times larger than $W_{0 \rightarrow 5g}$, which is due to the n-doping of QD #5. In this work, $W_{0 \rightarrow 1g} = 9.5 \times 10^{13} \text{ s}^{-1}$ and $W_{5g \rightarrow 0} = 2.0 \times 10^{14} \text{ s}^{-1}$. These fast transitions are achieved through two factors: the DOS of the NR and the n-doping of the "zero-region" and QD #5. Another contributing factor is the QDs' eigenenergies relative to each other, i.e. if any of the QD's energy level is modified, without adjusting the other QDs' eigenenergies, the trapping efficiency will decrease. Furthermore, the central QD's eigenenergy is the second lowest among all QDs. Based on the geometry and the dimensions of the QDs, the energy difference between the central QD's eigenenergy and the neighbor QDs' eigenenergies is almost 65 meV. This means the trapped electron needs to absorb two LO phonons in addition to a LA phonon to be able to escape. In order for the trapped electron to escape to QD #5 ground state, an energy difference of 86 meV needs to be overcome by the emission of at least two LO phonons and one LA phonon. Even with strong ELOPI, these processes take more than 1 ns.³⁴

Once the electron gets injected from the "zero-region" to the QD#1, it keeps hopping among the five QDs. As shown in Sec. IV, both t_{21} and t_{54} are of the order of 170 meV, which means the electron hopping is faster than the phonons' response. However, due to the presence of the *electron pocket*, i.e. $t_{42} > t_{43} + t_{32}$, the electron hops faster between QD #2 and QD #4 than hopping between QD #2 and QD #3. Therefore electron trapping due to detuning is excluded. Meanwhile, due to the relatively smaller value of t_{43} and t_{32} , part of electron's

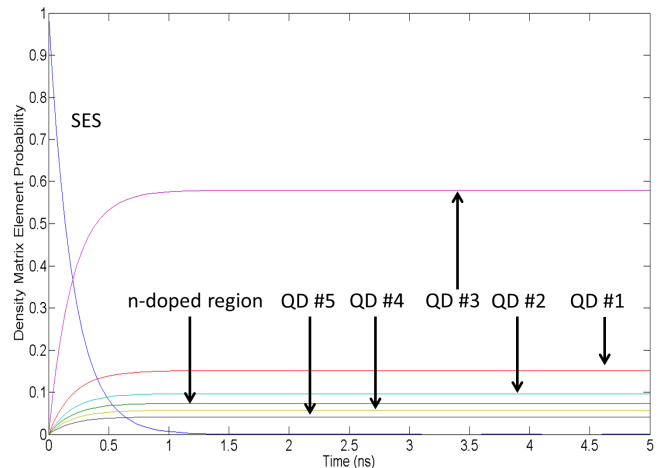


Figure 7: The electron's time-dependent probability distribution among the five quantum dots at 300 K. The probability to trap the electron in QD #3 is 58%.

wavefunction slowly keeps accumulating inside QD #3, while the rest of the electron's wavefunction hops to QD #4, from QD #2 then quickly to QD #5, and then to the "zero-region", from which it hops back to QD #1. The revolved part of the electron's wavefunction interferes constructively with the part that remained in the electron-pocket, leading to the localization of the electron. However, the localized electron will not stay inside QD #3 forever because both t_{43} and t_{32} are not zero. If there is no decoherence, the electron will hop out from QD #3 leaving behind 27% probability of trapping. The trapping probability depends on when the decoherence will terminate the hopping, i.e. off-diagonal terms, between QDs. At 100 K, the electron gets accumulated inside QD #3, before the electron starts to hop out of QD #3, the decoherence destroys the electron's hopping, hence the electron is trapped with a trapping probability of 70%. At 300 K, decoherence is much faster than at 100 K. While the electron is accumulated inside QD #3, the decoherence inhibits further accumulation. Thus the trapping efficiency decreases to 58%. The whole mechanism is based on a configuration that localizes the electron inside QD #3 through constructive quantum interference of the electron with itself and by means of decoherence that prevents the electron from hopping out. Therefore, trapping an electron inside QD #3 requires a delicate balance between how fast the electron is accumulated versus how large the decoherence rate is. Such a physical mechanism should manifest itself through oscillations in the diagonal density matrix elements in Fig. 12. The absence of oscillations due to the above explanation is attributed to the strong damping of the decoherence. This means the time evolution is dominated by overdamping. However, compare this results with the result obtained in App. D, when the electron's initial state is $|1g, 0\rangle$ instead of $|SES\rangle$. In that case the oscillations reflecting the electron's dynamics are visible and clearly

as shown in Fig. 12.

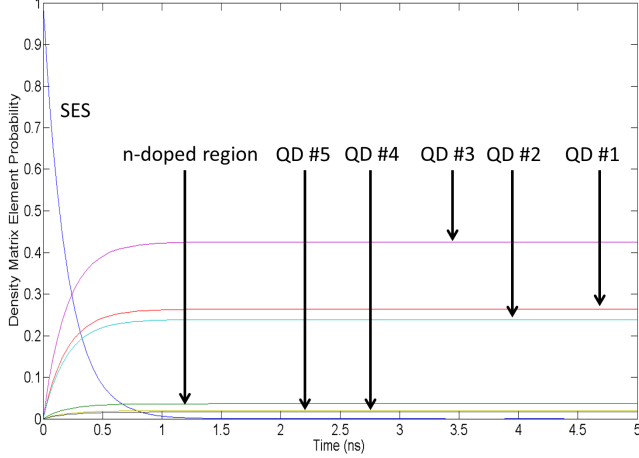


Figure 8: The electron's time-dependent probability distribution among the five quantum dots, at $T = 300$ K *without* electron pocket.

VII. CONCLUSION

We propose a realistic configuration to trap an electron at high temperature (100 K - 300 K) by taking advantage of the interplay between quantum interference and decoherence in an electron-pocket configuration. We would like to emphasize that the electron trapping takes place as a result of the interplay of both decoherence and quantum interference. Neither quantum interference nor decoherence alone can achieve electron trapping. In addition, as mentioned previously, the electron will require two LO phonons in addition to one LA phonon to be able to escape to the other QDs. The trapping is achieved with a probability ρ_{33} depending on the temperature. At $T = 100$ K, 200 K, 300 K the trapping probability is $\rho_{33} = 70\%$, 63%, and 58%, respectively.

Acknowledgments

We acknowledge support from NSF (Grant No. ECCS-0725514), DARPA/MTO (Grant No. HR0011-08-1-0059), NSF (Grant No. ECCS-0901784), AFOSR (Grant No. FA9550-09-1-0450), and NSF (Grant No. ECCS-1128597). We thank Winston Schoenfeld, Volodymyr Turkowski, and Mikhail Erementchouk for useful discussions.

Appendix A: Electron-Phonon Interaction in Quantum Dots

The Fröhlich Hamiltonian describes the electron-LO phonons interaction (ELOPI). For quantum dots (QDs),

it is given by

$$H_{e-ph} = \frac{1}{\sqrt{V}} \sum_{\mathbf{q}, i, j} M_{\mathbf{q}, i, j} a_i^\dagger a_j (b_{\mathbf{q}}^\dagger + b_{-\mathbf{q}}), \quad (\text{A1})$$

$$M_{\mathbf{q}, i, j} = i\sqrt{4\alpha} \frac{\hbar\omega_{\mathbf{q}}}{q} \left(\frac{\hbar}{2m^*\omega_{\mathbf{q}}} \right)^{1/4} \langle i | e^{i\mathbf{q}\cdot\mathbf{r}} | j \rangle, \quad (\text{A2})$$

where α is the Fröhlich coupling constant. In bulk InAs $\alpha = 0.052$. However, in InAs QDs $\alpha = 0.15$.^{35,36} $|i\rangle$ is the wavefunction for the electron level i in the QD. V is the volume of the NR. The phonons are assumed to be the same as those in the bulk $\text{In}_{0.45}\text{Ga}_{0.55}\text{As}$, since 85% of the NR is made of $\text{In}_{0.45}\text{Ga}_{0.55}\text{As}$. In this work, the LO phonons are regarded as dispersionless, i.e. $\hbar\omega_{\mathbf{q}} = \hbar\omega_{LO} = 32$ meV. We calculate the strength of couplings, in each QD, for the following cases: $|i\rangle = |j\rangle = |g\rangle$, $|i\rangle = |j\rangle = |e\rangle$, and $(|i\rangle = |g\rangle \text{ and } |j\rangle = |e\rangle)$, where $|g\rangle$ ($|e\rangle$) is the ground (excited) state. The coupling strength in Eq. (2) is calculated as follows:

$$\begin{aligned} \lambda^2 &= \sum_{|\mathbf{q}| \leq 2\pi/L} |\lambda_{\mathbf{q}}|^2 \\ &= \frac{1}{V} \sum_{|\mathbf{q}| \leq 2\pi/L} |M_{\mathbf{q}, i, j}|^2. \end{aligned} \quad (\text{A3})$$

For both $M_{\mathbf{q}, g, g}$ and $M_{\mathbf{q}, e, e}$, in all five QDs, $g = \lambda/(\hbar\omega_{LO}) = 0.066$. Consequently, $e^{-2g^2} \approx 1$. As for $M_{\mathbf{q}, g, e}$ or $M_{\mathbf{q}, e, g}$, in all five QDs, they are almost 0.0066.

Appendix B: Energy levels and wavefunctions of cylindrical QDs

As shown in Fig. 1, the "intrinsic-region" constitutes 15% of the NR. In addition, the "intrinsic-region" is along the z -axis. In this work, we consider the "intrinsic-region" curvature to be small. Thus, the "intrinsic-region" will be treated without curvature. Starting with Schrödinger's equation in cylindrical coordinates

$$\begin{aligned} E\Psi(\rho, \phi, z) &= -\frac{\hbar^2}{2m^*} \left[\frac{1}{\rho} \partial_\rho (\rho \partial_\rho \Psi(\rho, \phi, z)) \right. \\ &\quad \left. + \frac{1}{\rho^2} \partial_{\phi\phi} \Psi(\rho, \phi, z) + \partial_{zz} \Psi(\rho, \phi, z) \right] \\ &\quad + V(\rho, \phi, z) \Psi(\rho, \phi, z), \end{aligned} \quad (\text{B1})$$

where $E = E_\rho + E_z$ is the total eigenenergy of the electron. Applying separation of variables, the azimuthal differential equation and its normalized solution will be

$$\partial_{\phi\phi} \Phi(\phi) + m^2 \Phi(\phi) = 0, \quad (\text{B2})$$

and

$$\Phi(\phi) = \frac{1}{\sqrt{2\pi}} e^{+im\phi}, \quad (\text{B3})$$

where m is the azimuthal quantum number. As for the axial differential equation, it is as follows

$$-\frac{\hbar^2}{2m^*}Z(z) + V(z) = E_z Z(z). \quad (\text{B4})$$

The solution for the axial equation is shown later. As for the radial differential equation, it is given by

$$\partial_{\rho\rho}R(\rho) + \frac{1}{\rho}\partial_{\rho}R(\rho) + \left(k_{\rho}^2 - \frac{m^2}{\rho^2}\right)R(\rho) = 0. \quad (\text{B5})$$

The general solution for the radial differential equation is

$$R(\rho) = C_1 J_m(k_{\rho}\rho) + C_2 N_m(k_{\rho}\rho), \quad (\text{B6})$$

where J_m is the Bessel function of the first kind and N_m is the Bessel function of the second kind. In this work, not all QDs share the same boundary conditions, i.e. *electron pocket*. Both QD #1 and #5 do not share an interface with the *electron pocket*. Thus at $\rho = 0$, $R(\rho)$ is finite, i.e. $C_2 = 0$. For both QD #1 and #5, at $\rho = r$, $R(\rho)$ is equal to zero. In order to satisfy this boundary condition, $k_{\rho} = \frac{\alpha_{mn}}{r}$. The radial wavefunction, for both QD #1 and #5, is

$$R(\rho) = C_1 J_m\left(\frac{\alpha_{mn}\rho}{r}\right). \quad (\text{B7})$$

The energy of the electron inside either QD #1 or QD #5 is the sum of the radial energy and the axial energy.

$$E = E_{\rho} + E_z. \quad (\text{B8})$$

The axial energy will be explored in details in App. C. As for the radial energy, it is as follows

$$E_{\rho} = \frac{\hbar^2 \alpha_{mn}^2}{2m^* r^2}. \quad (\text{B9})$$

C_1 is determined from the normalization condition as follows

$$|C_1|^2 \int_0^{\rho=r} \rho \left| J_m\left(\frac{\alpha_{mn}\rho}{r}\right) \right|^2 d\rho = 1. \quad (\text{B10})$$

As for QD #2 and #4, both are identical.

For $\rho < \gamma r$, the electron's energy is denoted by E_{in} , where $E_{in} = E_{\rho in} + E_{z in}$, while for $\rho > \gamma r$, the electron's energy is denoted by E_{out} , where $E_{out} = E_{\rho out} + E_{z out}$. Based on Fig. 9, the boundary conditions are as follows:

1. at $\rho = 0$, $R(\rho)$ is finite.
2. at $\rho = \gamma r$, $R_{in}(\rho) = R_{out}(\rho)$.
3. at $\rho = \gamma r$, $\frac{dR_{in}(\rho)}{d\rho} = \frac{dR_{out}(\rho)}{d\rho}$.
4. at $\rho = r$, $R_{out}(\rho) = 0$.
5. Normalization condition: $|\langle R|R \rangle|^2 = 1$.

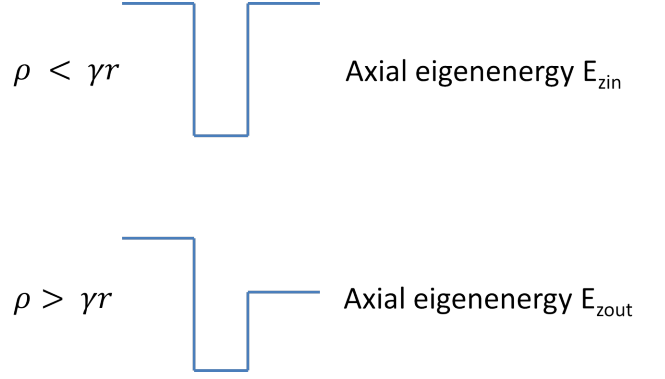


Figure 9: Schematic for the QD #2 or #4 interface with the electron pocket.

6. $E_{in} = E_{out}$.

γ is a constant factor that varies between 0 and 1. We set γ to be 0.533. The choice for γ is based on two factors. First, it is chosen to increase the efficiency of trapping by making t_{42} larger than $t_{32} + t_{43}$. Second, the value of γ makes the energy separation between the ground state's energy of QD #2 or #4 almost 70 meV higher than the ground state's energy of QD #3. Hence it takes the trapped electron almost 1 ns to escape. For $\rho < \gamma r$, the radial differential equation is

$$\partial_{\rho\rho}R(\rho) + \frac{1}{\rho}\partial_{\rho}R(\rho) + \left(k_{\rho in}^2 - \frac{m^2}{\rho^2}\right)R(\rho) = 0, \quad (\text{B11})$$

where $E_{\rho in} = \frac{\hbar^2 k_{\rho in}^2}{2m^*}$. The general solution for Eq. (B11), is

$$R_{in}(\rho) = C_3 J_m(k_{\rho in}\rho) + C_4 N_m(k_{\rho in}\rho). \quad (\text{B12})$$

From boundary condition 1, C_4 is zero. For $\rho > \gamma r$, the radial differential equation is

$$\partial_{\rho\rho}R(\rho) + \frac{1}{\rho}\partial_{\rho}R(\rho) + \left(k_{\rho out}^2 - \frac{m^2}{\rho^2}\right)R(\rho) = 0, \quad (\text{B13})$$

where $E_{\rho out} = \frac{\hbar^2 k_{\rho out}^2}{2m^*}$. The general solution for Eq. (B13), is

$$R_{out}(\rho) = C_5 J_m(k_{\rho out}\rho) + C_6 N_m(k_{\rho out}\rho). \quad (\text{B14})$$

Both R_{in} and R_{out} share the same "m". From boundary condition 4,

$$C_6 = -C_5 \frac{J_m(k_{\rho out}r)}{N_m(k_{\rho out}r)}. \quad (\text{B15})$$

From both boundary conditions 2 and 3, and simple algebraic manipulation, the transcendental equation reads

$$\begin{aligned} & k_{\rho out} J_m(k_{\rho in}\gamma r) \left[J'_m(k_{\rho out}\gamma r) N_m(k_{\rho out}\gamma r) \right. \\ & \left. - J_m(k_{\rho out}\gamma r) N'_m(k_{\rho out}\gamma r) \right] \\ & = k_{\rho in} J'_m(k_{\rho in}\gamma r) [J_m(k_{\rho out}\gamma r) N_m(k_{\rho out}r) \\ & \quad - J_m(k_{\rho out}r) N_m(k_{\rho out}\gamma r)]. \end{aligned} \quad (\text{B16})$$

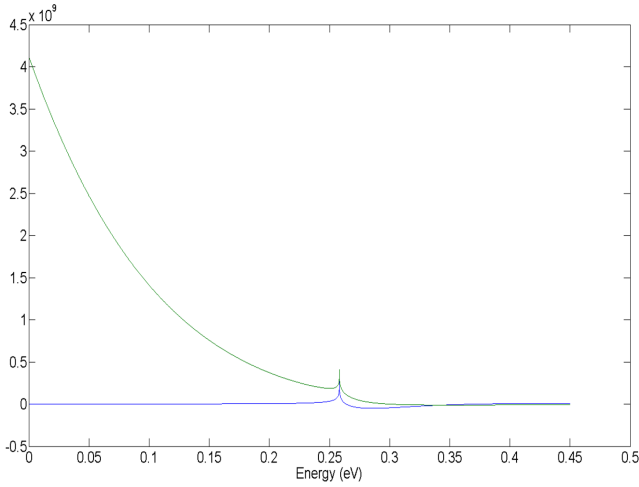


Figure 10: The solution for the transcendental equation.

As shown in Fig. 10, the solution for this transcendental equation, with $\gamma = 0.533$, is $E = 0.348$ eV. QD #3 is treated the same as both QD #1 and #5, but with different radius.

Appendix C: The axial energy levels of the cylindrical QDs

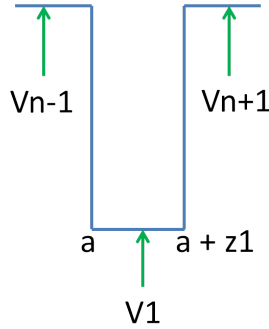


Figure 11: Schematic for the QD's height.

We write down the solution for Schrödinger's non-relativistic time-independent equation for the QD's different regions along the z -axis, for $-\infty < z < a$,

$$Z_1(z) = Ae^{k_{n-1}(z-a)}, \quad (C1)$$

for $a < z < a + z_1$,

$$Z_2(z) = B \cos(k_n(z-a)) + C \sin(k_n(z-a)), \quad (C2)$$

where z_1 is the height of the QD. For $a + z_1 < z < \infty$,

$$Z_1(z) = De^{-k_{n+1}(z-a)}. \quad (C3)$$

From the boundary conditions at $z = a$, we obtain

$$B = A, \quad (C4)$$

$$C = \sigma_1 A, \quad (C5)$$

where $\sigma_1 = \frac{m_n k_{n-1}}{m_{n-1} k_n}$. From the boundary conditions at $z = a + z_1$, we get

$$B \cos(k_n z_1) + C \sin(k_n z_1) = De^{-k_{n+1}(z_1)} \quad (C6)$$

and

$$-\frac{k_n}{m_n} B \sin(k_n z_1) + \frac{k_n}{m_n} C \cos(k_n z_1) = -\frac{k_{n+1}}{m_{n+1}} De^{-k_{n+1}(z_1)}. \quad (C7)$$

From Eq. (C1) and Eq. (C2), Eq. (C3) and Eq. (C5) yield, respectively,

$$A \cos(k_n z_1) + \sigma_1 A \sin(k_n z_1) = De^{-k_{n+1}(z_1)}, \quad (C8)$$

and

$$-A \sin(k_n z_1) + \sigma_1 A \cos(k_n z_1) = -\sigma_2 De^{-k_{n+1}(z_1)}, \quad (C9)$$

where $\sigma_2 = \frac{m_n k_{n+1}}{m_{n+1} k_n}$. After getting rid of A by dividing Eq. (C8) by Eq. (C9) and using a few straightforward algebraic steps, the transcendental equation for the QD eigenenergies is

$$\tan(k_n z_1) = \frac{\sigma_2 + \sigma_1}{1 - \sigma_1 \sigma_2}. \quad (C10)$$

A graphical solution provides the eigenenergies for each QD.

Going back to Eq. (C8) and Eq. (C9), D in terms of A is given by

$$D = \frac{\sigma_1^2 + 1}{\sigma_1 + \sigma_2} \sin(k_n z_1) e^{k_{n+1}(z_1)} A. \quad (C11)$$

After normalization, we obtain $A = 1/\sqrt{N}$, where

$$N = \frac{1}{2k_{n-1}} + \left(\frac{\sigma_1^2 + 1}{\sigma_1 + \sigma_2} \right)^2 \sin^2(k_n z_1) \frac{1}{2k_{n+1}} + \frac{1}{4k_n} (2k_n z_1 + \sin(2k_n z_1)) + \sigma_1^2 \left(\frac{z_1}{2} - \frac{\sin(2k_n z_1)}{4k_n} \right) - \frac{\sigma_1}{2k_n} (\cos(2k_n z_1) - 1). \quad (C12)$$

Appendix D: Electron's oscillations among the five quantum dots

In this appendix we change the initial condition from $\rho_{SES} = 1$ to $\rho_{11} = 1$. The reason is to illustrate the oscillations that are suppressed by decoherence if the initial

condition is $\rho_{SES} = 1$. In Fig. 12 oscillations due to interference are clearly visible. Note that despite the change in the initial condition, the results are the same. In addition, the time scale here is in the picosecond regime, while the timescale for the previous results is in the nanosecond regime. The reason is that the injection rate from the SES to the NR is $5 \times 10^9 \text{ s}^{-1}$.

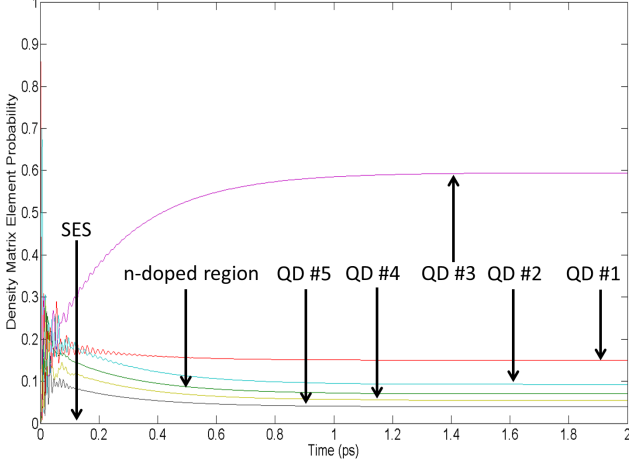


Figure 12: The electron's time-dependent probability distribution among the five quantum dots at room temperature with $\rho_{11} = 1$ as initial condition.

Appendix E: Approximation of the hopping matrix elements

As an illustration, in this appendix we are going to generalize the 1D calculation of the hopping matrix elements for a symmetric double-well potential presented in Ref. 37 to the case of an asymmetric double-well potential. We emphasize that we do not use this approximation in the calculations. This appendix is provided for educational purpose only. The effective Hamiltonian for a coupled two-level system is

$$H = \begin{pmatrix} \epsilon & t \\ t & -\epsilon \end{pmatrix}, \quad (\text{E1})$$

where 2ϵ is the bias between the right and left well, and t is the hopping matrix element. The eigenenergies are $E_{\pm} = \sqrt{\epsilon^2 + t^2}$. The corresponding eigenstates are

$$|\psi_+\rangle = \cos \frac{\theta}{2} |\psi_R\rangle + \sin \frac{\theta}{2} |\psi_L\rangle, \quad (\text{E2})$$

$$|\psi_-\rangle = -\sin \frac{\theta}{2} |\psi_R\rangle + \cos \frac{\theta}{2} |\psi_L\rangle, \quad (\text{E3})$$

where $\tan \theta = t/\epsilon$ with $0 \leq \theta < \pi$. For determining E_+ we use the following two Schrödinger equations:

$$\psi_R'' + \frac{2m}{\hbar^2} (E_R - V) \psi_R = 0, \quad (\text{E4})$$

$$\psi_+'' + \frac{2m}{\hbar^2} (E_+ - V) \psi_+ = 0, \quad (\text{E5})$$

where V is the 1D potential shown in Fig. 13. Multiplying ψ_+ to Eq. (E4), multiplying ψ_R to Eq. (E5), and taking the difference results in

$$\psi_+ \psi_R'' - \psi_R \psi_+'' + \frac{2m}{\hbar^2} (E_R - E_+) \psi_R \psi_+ = 0 \quad (\text{E6})$$

After integration from 0 to infinity and integration by parts, we obtain

$$E_+ - E_R = \frac{\hbar^2}{2m\delta_{R,+}^+} [-\psi_+(0)\psi_R'(0) + \psi_R(0)\psi_+'(0)], \quad (\text{E7})$$

where $\delta_{R,+}^+ = \int_0^\infty \psi_R \psi_+ dx$.

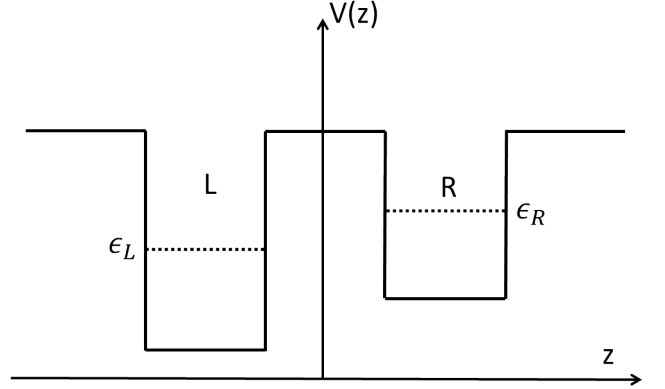


Figure 13: Schematic showing an asymmetric double well potential.

A similar calculation can be done for determining $E_- - E_R$. Evaluating the difference, we obtain

$$E_- - E_+ = \frac{\hbar^2}{2m\delta_{R,-}^+} [-\psi_+(0)\psi_L'(0) + \psi_L(0)\psi_+'(0)] - \frac{\hbar^2}{2m\delta_{R,+}^+} [-\psi_+(0)\psi_R'(0) + \psi_R(0)\psi_+'(0)], \quad (\text{E8})$$

where $\delta_{L,+}^+ = \int_0^\infty \psi_L \psi_+ dx$. Using the approximations $\delta_{R,-}^+ \approx -\sin \frac{\theta}{2}$ and $\delta_{R,+}^+ \approx \cos \frac{\theta}{2}$, we can substantially simplify the above equation to

$$E_- - E_+ = \frac{\hbar^2}{2m} \left[\cot \frac{\theta}{2} + \tan \frac{\theta}{2} \right] \times [\psi_L(0)\psi_R'(0) - \psi_L'(0)\psi_R(0)]. \quad (\text{E9})$$

Using the formulas $\tan \frac{\theta}{2} = \frac{1-\cos \theta}{\sin \theta}$ and $\cot \frac{\theta}{2} = \frac{1+\cos \theta}{\sin \theta}$, we obtain

$$E_- - E_+ = \frac{\hbar^2 k^2}{m \sin \theta} = 2\sqrt{\epsilon^2 + t^2}, \quad (\text{E10})$$

where we defined $k^2 = [\psi_L(0)\psi_R'(0) - \psi_L'(0)\psi_R(0)]$. Since $\sin \theta = t/\sqrt{\epsilon^2 + t^2}$, we get

$$t = \frac{\hbar^2 k^2}{2m}. \quad (\text{E11})$$

We compared this approximation with the result obtained using Eq. (18). Our calculations show that this approximation gives less than 50% of the kinetic matrix element in Eq. (18) and less than 40% of the total matrix element in Eq. (18). This discrepancy is due to the

approximations $\delta_{R,-}^+ \approx -\sin \frac{\theta}{2}$ and $\delta_{R,+}^+ \approx \cos \frac{\theta}{2}$, which neglect the tails of the wavefunctions. This result illustrates also the importance of including the off-diagonal matrix elements of the potential.

-
- * Electronic address: Michael.Leuenberger@ucf.edu
- ¹ H.-P. Breuer and F. Petruccione, *The Theory of Open Quantum Systems* (Oxford University Press, New York, 2002).
 - ² J. Fischer and D. Loss, *Science* **324**, 1277 (2009).
 - ³ S. Deleglise, I. Dotsenko, C. Sayrin, J. Bernu, M. Brune, J.-M. Raimond, and S. Haroche, *Nature* **455**, 510 (2008).
 - ⁴ A. van Oudenaarden, M. Devoret, Y. Nazarov, and J. Mooij, *Nature* **391**, 768 (1998).
 - ⁵ A. Bachtold, C. Strunk, J. Salvetat, J. Bonard, L. Forro, T. Nussbaumer, and C. Schonenberger, *Nature* **397**, 673 (1999).
 - ⁶ J. R. Anglin, J. P. Paz, and W. H. Zurek, *Phys. Rev. A* **55**, 4041 (1997).
 - ⁷ P. W. Shor, *Phys. Rev. A* **52**, R2493 (1995).
 - ⁸ H. Bluhm, S. Foletti, I. Neder, M. Rudner, D. Mahalu, V. Umansky, and A. Yacoby, *Nat. Phys.* **7**, 109 (2011).
 - ⁹ J. Petta, A. Johnson, J. Taylor, E. Laird, A. Yacoby, M. Lukin, C. Marcus, M. Hanson, and A. Gossard, *Science* **309**, 2180 (2005).
 - ¹⁰ H. Rabitz, R. de Vivie-Riedle, M. Motzkus, and K. Kompa, *Science* **288**, 824 (2000).
 - ¹¹ G. A. Álvarez and D. Suter, *Phys. Rev. Lett.* **107**, 230501 (2011).
 - ¹² M. Mohseni, P. Rebentrost, S. Lloyd, and A. Aspuru-Guzik, *J. Chem. Phys.* **129** (2008).
 - ¹³ F. Caruso, A. W. Chin, A. Datta, S. F. Huelga, and M. B. Plenio, *J. Chem. Phys.* **131** (2009).
 - ¹⁴ M. B. Plenio and S. F. Huelga, *New J. Phys.* **10** (2008).
 - ¹⁵ F. L. Semiao, K. Furuya, and G. J. Milburn, *New J. Phys.* **12** (2010).
 - ¹⁶ S. Lloyd and M. Mohseni, *New J. Phys.* **12** (2010).
 - ¹⁷ C. K. J. K. I.-O. S. D. Giulini, E. Joos and H. D. Zeh, *Decoherence and the Appearance of a classical World in Quantum Theory* (Springer, New York, 1996).
 - ¹⁸ G. A. Álvarez and D. Suter, *Phys. Rev. A* **84**, 012320 (2011), URL <http://link.aps.org/doi/10.1103/PhysRevA.84.012320>.
 - ¹⁹ M. B. and S. C. G., *J. Math. Phys.* **18**, 756 (1977), URL <http://jmp.aip.org/>.
 - ²⁰ B. Kaulakys and V. Gontis, *Phys. Rev. A* **56**, 1131 (1997), URL <http://link.aps.org/doi/10.1103/PhysRevA.56.1131>.
 - ²¹ G. Feve, A. Mahe, J. M. Berroir, T. Kontos, B. Placais, D. C. Glattli, A. Cavanna, B. Etienne, and Y. Jin, *Science* **316**, 1169 (2007).
 - ²² E. Bocquillon, F. D. Parmentier, C. Grenier, J.-M. Berroir, P. Degiovanni, D. C. Glattli, B. Placais, A. Cavanna, Y. Jin, and G. Fève, *Phys. Rev. Lett.* **108**, 196803 (2012).
 - ²³ M. A. Omar, *Elementary Solid State Physics* (Addison-Wesley Publishing Company, Massachusetts, 1975).
 - ²⁴ T. Inoshita and H. Sakaki, *Phys. Rev. B* **56**, R4355 (1997), URL <http://link.aps.org/doi/10.1103/PhysRevB.56.R4355>.
 - ²⁵ E. Stock, M.-R. Dachner, T. Warming, A. Schliwa, A. Lochmann, A. Hoffmann, A. I. Toropov, A. K. Bakarov, I. A. Derebezov, M. Richter, et al., *Phys. Rev. B* **83**, 041304 (2011), URL <http://link.aps.org/doi/10.1103/PhysRevB.83.041304>.
 - ²⁶ K. E. Cahill and R. J. Glauber, *Phys. Rev.* **177**, 1857 (1969), URL <http://link.aps.org/doi/10.1103/PhysRev.177.1857>.
 - ²⁷ K. E. Cahill and R. J. Glauber, *Phys. Rev.* **177**, 1882 (1969), URL <http://link.aps.org/doi/10.1103/PhysRev.177.1882>.
 - ²⁸ K. Blum, *Density Matrix Theory and Applications* (Plenum Press, New York, 1996).
 - ²⁹ P. Borri, W. Langbein, J. Mørk, J. M. Hvam, F. Heinrichsdorff, M.-H. Mao, and D. Bimberg, *Phys. Rev. B* **60**, 7784 (1999).
 - ³⁰ A. V. Uskov, A.-P. Jauho, B. Tromborg, J. Mørk, and R. Lang, *Phys. Rev. Lett.* **85**, 1516 (2000), URL <http://link.aps.org/doi/10.1103/PhysRevLett.85.1516>.
 - ³¹ P. Borri, W. Langbein, S. Schneider, U. Woggon, R. L. Sellin, D. Ouyang, and D. Bimberg, *Phys. Rev. Lett.* **87**, 157401 (2001), URL <http://link.aps.org/doi/10.1103/PhysRevLett.87.157401>.
 - ³² S. Sauvage, P. Boucaud, R. P. S. M. Lobo, F. Bras, G. Fishman, R. Prazeres, F. Glotin, J. M. Ortega, and J.-M. Gérard, *Phys. Rev. Lett.* **88**, 177402 (2002), URL <http://link.aps.org/doi/10.1103/PhysRevLett.88.177402>.
 - ³³ J. Singh, *Electronic and Optoelectronic Properties of Semiconductor Structures* (Cambridge, Cambridge, 2003).
 - ³⁴ T. Inoshita and H. Sakaki, *Phys. Rev. B* **46**, 7260 (1992), URL <http://link.aps.org/doi/10.1103/PhysRevB.46.7260>.
 - ³⁵ R. Heitz, I. Mukhametzhanov, O. Stier, A. Madhukar, and D. Bimberg, *Phys. Rev. Lett.* **83**, 4654 (1999).
 - ³⁶ M. A. Odnoblyudov, I. N. Yassievich, and K. A. Chao, *Phys. Rev. Lett.* **83**, 4884 (1999).
 - ³⁷ L. D. Landau and E. M. Lifshitz, *Quantum Mechanics: Non-Relativistic Theory* (Oxford University Press, New York, 1977).